JACS
JOURNAL OF THE AMERICAN CHEMICAL SOCIETY

Article

pubs.acs.org/JACS

Structural Characterization of Dihydrofolate Reductase Complexes by Top-Down Ultraviolet Photodissociation Mass Spectrometry

Michael B. Cammarata,[†] Ross Thyer,[‡] Jake Rosenberg,[†] Andrew Ellington,[‡] and Jennifer S. Brodbelt*[,†]

[†]Department of Chemistry and [‡]Center for Systems and Synthetic Biology, University of Texas at Austin, Austin, Texas 78712, United States

Supporting Information

ABSTRACT: The stepwise reduction of dihydrofolate to tetrahydrofolate entails significant conformational changes of dihydrofolate reductase (DHFR). Binary and ternary complexes of DHFR containing cofactor NADPH, inhibitor methotrexate (MTX), or both NADPH and MTX were characterized by 193 nm ultraviolet photodissociation (UVPD) mass spectrometry. UVPD yielded over 80% sequence coverage of DHFR and resulted in production of fragment ions that revealed the interactions between DHFR and each ligand. UVPD of the binary DHFR·NADPH and DHFR·MTX complexes led to an unprecedented number of fragment ions containing either an N- or C-terminal protein fragment still bound to the ligand via retention of noncovalent interactions. In addition, holo-fragments retaining both ligands were observed upon UVPD of the ternary DHFR·NADPH·MTX complex. The combination of extensive holo and apo fragment ions allowed the locations of the NADPH and MTX ligands to be mapped, with NADPH associated with the adenosine binding domain of DHFR and MTX interacting with the loop domain. These findings are consistent with previous crystallographic evidence. Comparison of the backbone cleavage propensities for apo DHFR and its holo counterparts revealed significant variations in UVPD fragmentation in the regions expected to experience conformational changes upon binding NADPH, MTX, or both ligands. In particular, the subdomain rotation and loop movements, which are believed to occur upon formation of the transition state of the ternary complex, are reflected in the UVPD mass spectra. The UVPD spectra indicate enhanced backbone cleavages in regions that become more flexible or show suppressed backbone cleavages for those regions either shielded by the ligand or involved in new intramolecular interactions. This study corroborates the versatility of 193 nm UVPD mass spectrometry as a sensitive technique to track enzymatic cycles that involve conformational rearrangements.

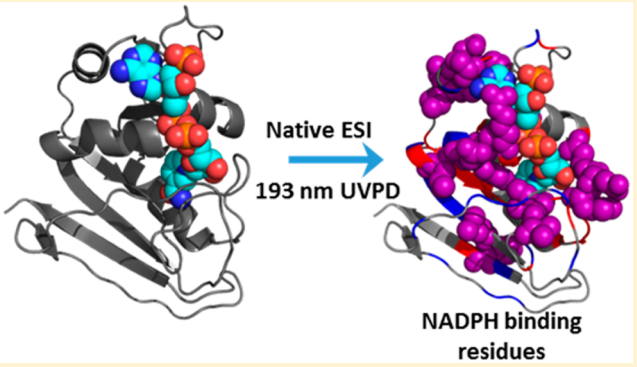

INTRODUCTION

The use of mass spectrometry in the field of structural biology has accelerated in recent years due to the advent of more effective means of transporting native-like proteins into the gas phase as well as refinement of methods used to probe protein structures such as hydrogen−deuterium exchange and tandem mass spectrometry.[1,2] Many of the original studies that explored the use of mass spectrometry for structural biology applications utilized covalent labeling or cross-linking of proteins and protein−ligand complexes in solution, followed by proteolytic digestion, separation, identification, and sometimes quantification of probe-modified or cross-linked peptides to reveal information about the solvent accessibility and interacting regions of the proteins.[1] More elegant strategies based on hydrogen−deuterium exchange of the protein backbone amide hydrogens have gained popularity due to their single residue resolution and sensitivity to conformational changes.[2] Most of these methods have utilized a bottom-up workflow in which the proteins of interest are enzymatically digested prior to analysis of the constituent peptides, thus providing an indirect means to correlate protein structure with peptide-level outcomes. Since the development of new, widely accessible high-performance mass spectrometers, there has been growing interest in employing top-down approaches for structural biology investigations, thus allowing evaluation of intact proteins transported to the gas phase.[3−25] Collisional, electron-based and photon-based activation methods have been used to analyze the intact proteins.[22,26−32] These methods have proven effective for quantifying covalent labeling or hydrogen−deuterium exchange of proteins to the same degree, if not more completely, than the corresponding bottom-up approaches on proteins below 30 kDa.[3−6,8,14]

Compelling new advances in the application of mass spectrometry to structural biology problems have been inspired by the recent successes in transporting presumed native-like proteins and protein complexes to the gas phase from buffered solutions via native spray methods.[11,33] This has opened up the

Received: May 5, 2015
Published: June 30, 2015

DOI: 10.1021/jacs.5b04628
J. Am. Chem. Soc. 2015, 137, 9128−9135

possibility of using mass spectrometry to directly interrogate native-like protein structures, primarily using MS/MS methods to disassemble the complexes, sequence the proteins, and draw conclusions about protein conformation based on fragmentation behavior.[10,11,15,21,22,34−39] One hallmark of native spray is the adoption of much lower charge states of the native-like proteins than those observed for denatured proteins sprayed from acidic, methanol-containing solutions. Although still a subject of debate, it is believed that proteins retain native-like conformations to a large extent, thus allowing examination binding interactions of protein complexes via an array of MS/MS methods.[11,20,21,40] Ion mobility mass spectrometry (IMMS) also plays a pivotal role in discerning and studying the three-dimensional shapes of proteins and protein complexes in the gas phase.[16,41] Collision-based activation of the resulting protein−ligand or protein−protein complexes leads to ejection of the ligands or intact protein monomers or multimers (from multimeric protein complexes) as well as some sequence ions from the proteins.[12,15,30] Activation of native-like proteins without any bound ligands leads to formation of sequence ions that have been correlated with the B-factors of the proteins and thus the local stabilities of specific regions.[15,34,42] Ultraviolet photodissociation (UVPD) in particular provides unsurpassed levels of sequence coverage for intact proteins (denatured ones)[26,27,43] and has more recently exhibited similar levels of performance for native-like proteins and protein complexes.[15,34] For the latter, UVPD resulted in conventional sequence ions for which the abundances of ions produced upon cleavage of inter-residue bonds mirrored the B-factors of the protein. In addition UVPD generated product ions comprised of a portion of the protein (*a*, *b*, *c*, *x*, *y*, or *z* ion) still bound through noncovalent interactions to the ligand.[15,44] One recent study showed that the abundance of the fragment ions from myoglobin varied as a function of heme binding (apo and holo states) in a way that aligned with expected conformational changes upon ligand binding.[34] Additionally it was recently reported that conformers of ubiquitin separated in the gas phase by ion mobility were differentiated based on their UVPD fragmentation patterns.[39] Electron-capture dissociation, electron-transfer dissociation, and surface-induced dissociation have also been used to disassemble native proteins or protein complexes in the gas phase.[20,22,36,45−48] Collectively, these studies have provided growing evidence that native spray, in conjunction with tandem mass spectrometry, can be employed to address increasingly advanced questions about the nature of protein−ligand interactions in the context of structural biology.[13,49] Herein we report the use of UVPD to examine binary and ternary protein ligand complexes, as described for dihydrofolate reductase (DHFR).

DHFR is a small protein (~19 kDa, 186 amino acids) that reduces dihydrofolate (DHF) to tetrahydrofolate (THF). THF is the precursor for all folate coenzymes involved in numerous biosynthetic pathways.[50,51] Nicotinamide adenine dinucleotide phosphate (NADPH) serves as a cofactor of DHFR during its catalytic cycle and is oxidized in the process.[52] The stepwise DHFR reaction has been explored by many methods to elucidate the energetics and structural intermediates.[51,53−57] An outstanding depiction of the dynamic landscape of DHFR catalysis and structural models of key intermediates in the catalytic cycle is provided in ref 56. There are two well-defined binding regions in DHFR: the adenosine-binding domain and the loop-binding domain.[51] Upon both substrate and cofactor binding, it has been established that there are specific loop movements, particularly in the M20, F-G and G-H loops, responsible for catalyzing the reduction of DHF and releasing THF and the oxidized NADP+.[51,53,57−59] These loop movements have been shown to be key conformational changes through the catalytic cycle. Additionally, DHFR plays a pivotal role in the folate cycle that produces thymine.[60] Thymine is required for the proliferation of rapidly dividing cells, such as those during cancerous metastasis. This feature makes DHFR a compelling drug target for the development of clinical therapeutics, such as methotrexate (MTX).[51,53,61,62] This potent inhibitor of DHFR has also been used in combination with NADPH to aide in the creation of models of the transition state of the DHFR reaction.[51] The fact that DHFR binds both NADPH and MTX makes it an attractive candidate for expanding the scope of UVPD for investigation of protein−ligand complexes. We report here that UVPD can be used to probe DHFR as well as its binary and ternary complexes (DHFR·NADPH, DHFR·MTX, and DHFR·NADPH·MTX) and to explore the stepwise impact of loop movements and the ligand binding sites as revealed by the UVPD fragmentation trends.

EXPERIMENTAL SECTION

DHFR Production. For expression of DHFR, the *E. coli folA* gene encoding dihydrofolate reductase including a C-terminal His6-tag (amplified from DH10B genomic DNA) was cloned into the NdeI/PacI sites of pETDuet-1 (Novagen). BL21(DE3) cells containing pETDuet-DHFR were cultured in 2 L of LB medium and induced with IPTG during mid log phase. Cells were harvested by centrifugation at 8000 × *g* for 10 min and resuspended in 20 mL of wash buffer (100 mM Tris, 150 mM NaCl, 1 mM EDTA at pH 8.0) with protease inhibitor cocktail (cOmplete, mini EDTA free, Roche) and lysozyme at 1 mg·mL^{-1}. Following a 20 min incubation at 4 °C cells were lysed by sonication (Model 500, Fisher Scientific) and clarified three times by centrifugation at 35000 × *g* for 30 min. Lysate was filtered through a 0.2 μm membrane, and DHFR was recovered by IMAC using Ni-NTA resin and gravity flow columns. Eluate was concentrated and dialyzed against 50 mM NH_4OAc pH 6.5, followed by purification to apparent homogeneity by size exclusion fast protein liquid chromatography (FPLC).

Mass Spectrometry. DHFR solutions were prepared by incubation of 15 μM DHFR stock in 50 mM ammonium acetate at pH 6.5 with 20× excess NADPH, MTX, or NADPH + MTX, respectively, for 30 min at room temperature. All ligands and reagents were obtained from Sigma-Aldrich. Each sample was cleaned six times with a 10 kDa molecular weight cutoff filter (Millipore, Darmstadt, Germany) and diluted to 7 μM with 50 mM ammonium acetate pH 6.5 for the native protein samples, while the denatured protein sample was filtered into 50:49:1 (water:acetonitrile:formic acid). Samples were infused using a 40 nm Au-coated static tip electrospray setup with an applied voltage of 1.2−1.5 kV. A heated capillary was set at 200 °C to assist desolvation of the proteins. All experiments were undertaken on a Thermo Scientific Instruments Orbitrap Elite mass spectrometer (Bremen, Germany) equipped with a Coherent Excistar excimer laser (Santa Cruz, CA) for photodissociation.[27] UVPD was performed in the HCD cell operated at 10 mTorr helium pressure and using a single 3.0 mJ laser pulse (193 nm wavelength) per spectrum. The 9+ charge-state species was selected in every case using an isolation width of 15 *m*/*z* and an AGC target of 1e5 with a maximum injection time of 1 s. 250 scans total were averaged for each spectrum.

Data Analysis. UVPD mass spectra were deconvoluted using the Thermo Xtract algorithm with a S/N ratio of 3, then searched through Prosight PC 3.0 modified with custom code to include nine UVPD-type ions (*a*, *a*•, *b*, *c*, *x*, *x*•, *y*, *y* − 1, *z*). These ion types are consistently found by UVPD.[27] The searches for and assignments of ligand-containing fragment ions (holo fragments in which a segment of the protein retains the ligand via noncovalent interactions) were done

DOI: 10.1021/jacs.5b04628
J. Am. Chem. Soc. 2015, 137, 9128−9135

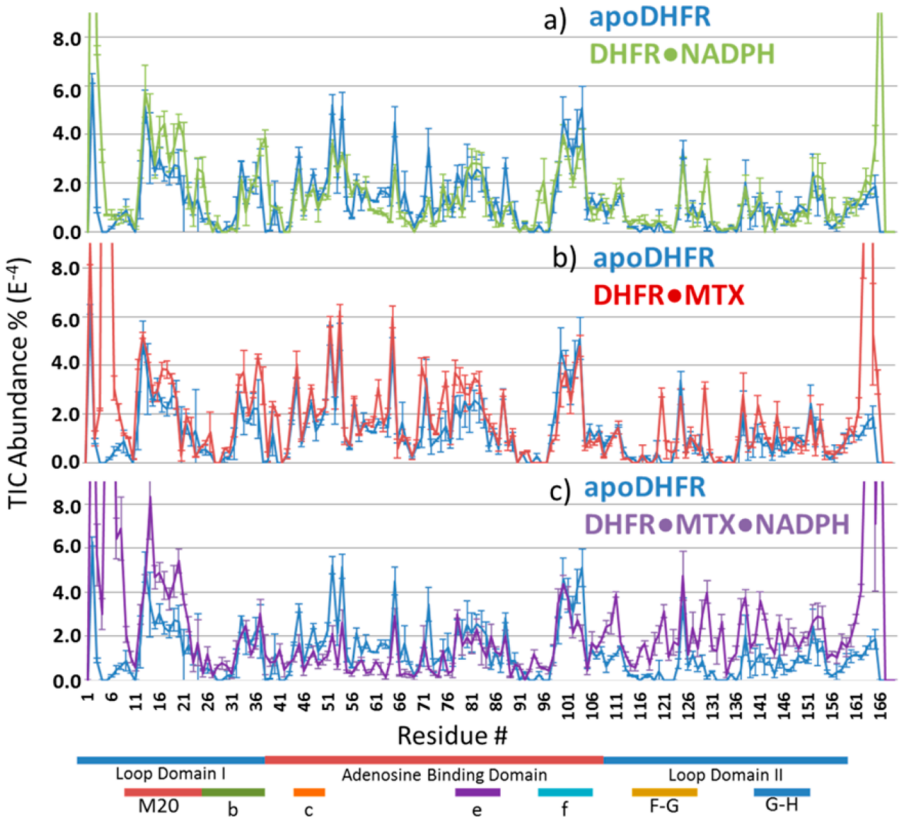

Figure 1. TIC abundance % per residue plots of summed holo + apo product ions (including both N- and C-termini ions) from DHFR and its respective complexes DHFR·NADPH (a), DHFR·MTX (b), and DHFR·NADPH·MTX (c). The 9+ charge state was selected for all experiments. The color code used for each protein is shown in the legend. Important structural features are highlighted below the graphs and relate directly to color coding in Supporting Information, Figure 1. Standard deviations were calculated from four replicates.

in a manner to account for mass shifts corresponding to retention of the MTX, NADPH, or MTX + NADPH ligands by the standard sequence ion types (*a*, *b*, *c*, *x*, *y*, and *z*). The ligand mass shifts plus up to three extra hydrogens (due to the prominence of hydrogen atom (not proton) migrations during activation of proteins by UVPD) were treated as variable modifications and were applied as follows: mass shift of 454.1713−457.1948 Da for MTX, 743.0750−746.09845 Da for NADPH, and 1198.2541−1201.2776 Da for MTX + NADPH. All identified ions were normalized relative to the total ion current of the respective spectra to allow evaluation of trends for all spectra. Fragment ions arising from cleavage of the backbone positions between pairs of adjacent amino acids in the protein sequence were collectively summed. For example, all product ions arising from backbone cleavages that occur N-terminal to a specific amino acid (yielding a_n, b_n, and c_n ions) were summed with all the complementary C-terminal product ions arising from the next flanking amino acid-containing backbone cleavage site (yielding complementary $x_{R-(n+1)}$, $y_{R-(n+1)}$, and $z_{R-(n+1)}$ ions), where R is the total number of amino acids in the protein. For visualization of the results, residues that displayed a significant change in fragmentation yields were highlighted on crystal structures representing DHFR·NADPH, DHFR·MTX, and DHFR·NADPH·MTX complexes. The PDB codes for these structures are 1RX1, 1RG7, and 1RX3, respectively. B-factors were extracted from the respective PDB files as well as for the apo-DHFR form from 5DFR. All visualizations were performed using Pymol 1.3 software. Pymol was also used to search for polar contacts with a 4.0 Å cutoff. All UVPD experiments were repeated at least three times. A structural representation of DHFR based on X-ray crystal structure 1RX3 is shown in Supporting Information, Figure 1, with the helices and binding domains labeled and color-coded.

RESULTS AND DISCUSSION

In this study, UVPD was used as a tool to characterize previously known ligand binding sites and evaluate changes in the structure of DHFR based are reflected by variations in the fragmentation patterns of the protein. DHFR was successfully transferred to the gas phase via native ESI conditions to generate apo and holo noncovalent complexes containing MTX, NADPH, or both NADPH and MTX in low-charge states (8+, 9+) characteristic of native-like proteins (Supporting Information, Figure 2). The 9+ charge state was the most abundant for each DHFR complex, and thus this charge state was isolated and subjected to UVPD for all MS/MS experiments. Examples of the resulting UVPD mass spectra are displayed in Supporting Information, Figure 3. Deconvolution shows that the UVPD spectra are very rich and high quality, containing a variety of multicharged *a*, *b*, *c*, *x*, *y*, *z* ions, some retaining the NADPH and/or MTX ligands (Supporting Information, Figures 3 and 4). In general *a*/*x*-type ions were about twice as abundant as *b*/*y* and *c*/*z* ions. UVPD of each of the native apo and holo proteins (9+) yielded at least 81% sequence coverage. For the native-like DHFR complexes, the pattern of backbone cleavages of DHFR (based on formation of N-terminal *a*, *b*, and *c* ions and C-terminal *x*, *y*, and *z* ions by UVPD) is influenced by the presence or absence of bound ligands as well as conformational changes that alter the flexibility/stability of specific regions and thus the susceptibility to fragmentation. The fact that absorption cross sections of proteins may vary with charge density or conformation has been postulated previously[63] and echoed in one of our previous

DOI: 10.1021/jacs.5b04628
J. Am. Chem. Soc. 2015, 137, 9128−9135

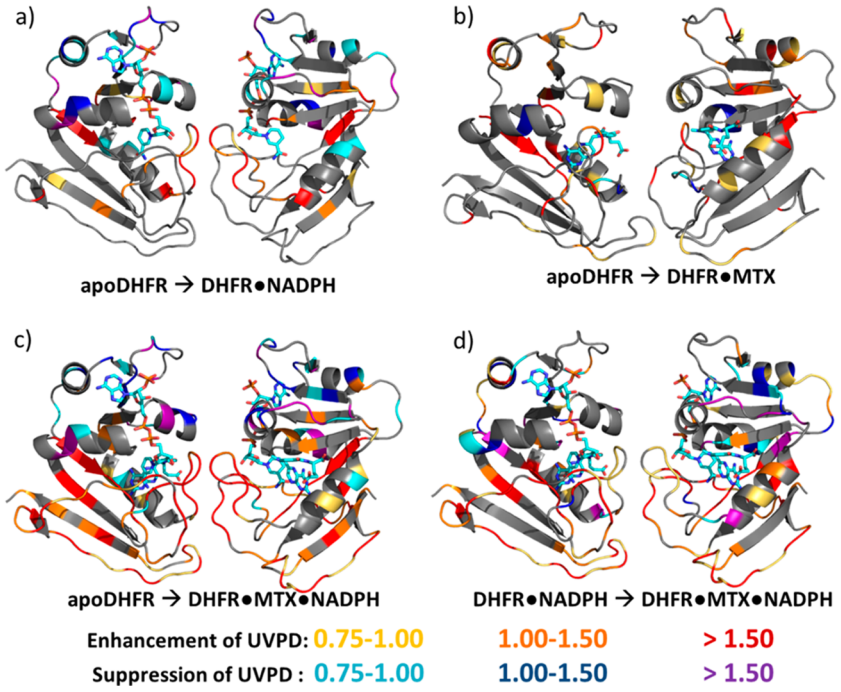

Figure 2. Those residues which had an enhanced (positive) or suppressed (negative) change in UVPD fragmentation upon comparison of apo-DHFR and (a) DHFR•NADPH, (b) DHFR•MTX, and (c) DHFR·MTX·NADPH as well as comparison of (d) DHFR•NADPH to DHFR·MTX·NADPH were highlighted according to the colored bins. In each case, the increase (enhancement) or decrease (suppression) in UVPD fragmentation yield is shown as a percentage representing the change in ion abundance (based on total ion current) and superimposed on the crystal structures. Crystal structures 1RX1, 1RG7, and 1RX3 were used to represent the DHFR•NADPH (a), DHFR• MTX (b), and DHFR·MTX·NADPH (c and d) complexes, respectively. Two 45° rotations are shown for each complex.

studies.[34] Variations in molar absorptivities of structural elements of proteins in solution (α-helices versus coiled/loop regions) have similarly been documented.[64]

The complexity of the UVPD mass spectra required careful analysis to differentiate and assign ligand-free (apo) and ligand-containing (holo) sequence ions, as described in the Experimental Section. For the ternary DHFR·NADPH·MTX complex, fragment ions containing either NAPDH or MTX or both NADPH and MTX were identified. The average numbers of ligand-containing fragment ions found for each DHFR complex are summarized in Supporting Information, Figure 5. The DHFR·MTX complex produced 46 unique MTX-containing fragment ions, and 135 unique NADPH-containing fragment ions were obtained from the DHFR·NADPH complex. For the multiligand ternary DHFR·NADPH·MTX complex, a total of 212 unique holo fragments were identified upon UVPD, including 106 retaining NADPH, 36 retaining MTX, and 70 containing both NADPH and MTX. In summary, NADPH was retained in a greater number of sequence ions than was MTX, and MTX was retained in more sequence ions for the ternary DHFR·NADPH·MTX complex than for the binary DHFR·MTX complex. In addition, NADPH was retained more frequently than MTX upon dissociation of the ternary DHFR·NADPH·MTX complex. In fact MTX was retained more often in conjunction with retention of NADPH than retention of MTX alone. This latter result suggested that the ternary DHFR·NADPH·MTX complex engaged in different and/or stronger interactions with the MTX ligand than found in the binary DHFR·MTX complex. The detection of sequence ions retaining both NADPH and MTX for the ternary DHFR·NADPH·MTX complex was particularly interesting, thus signaling the survival of the noncovalent interactions between the protein and two different ligands during the photoactivation and dissociation process.

Each UVPD mass spectrum was processed to calculate the relative fragmentation propensities between each pair of amino acids in the sequence (i.e., based on backbone cleavages between every pair of residues; summing those C-terminal *x*, *y*, *z* and N-terminal *a*, *b*, *c* ions surrounding each amino acid as described in the Experimental Section). The backbone cleavage propensities are summarized in graphical form in Figure 1, with the results for apo-DHFR overlaid with the corresponding results for each of the three complexes (DHFR·NADPH, DHFR·MTX, and DHFR·NADPH·MTX in Figure 1a–c, respectively). A number of notable differences were observed upon inspection of the fragmentation trends for apo-DHFR relative to its complexes: cleavage at some backbone sites was enhanced; others were significantly suppressed upon ligand binding. To aid in visualization of the regions of the protein for which fragmentation was enhanced or suppressed, the residues corresponding to those backbone cleavage sites are highlighted on the structures of the various DHFR complexes in Figure 2. The structural elements and subdomains of DHFR are illustrated in Supporting Information, Figure 1. Selected amino acids are numbered to facilitate visual orientation of the protein relative to the backbone sites for which cleavage is altered going from the apoprotein to the holo-protein complexes. In Figure 2, the change in fragmentation propensity for each DHFR complex is scaled relative to the fragmentation propensity of apo-DHFR. A decrease in backbone fragmentation (*suppression* of fragmentation) is highlighted in binned cool colors (cyan, blue, purple) on each crystal structure, and increases in backbone fragmentation (enhancement of fragmentation upon ligand binding) are binned into warm

DOI: 10.1021/jacs.5b04628
J. Am. Chem. Soc. 2015, 137, 9128–9135

colors (yellow, orange, red). For native-like proteins or protein−ligand complexes in the gas phase, the suppression or enhancement of specific backbone cleavage sites upon UVPD is modulated by two primary effects: shielding of backbone sites by noncovalent interactions with the ligands or involvement in other intramolecular interactions (thus suppressing fragmentation of those regions) or enhancement of backbone fragmentation due to increased conformational flexibility (higher B value).[15,34] Regions with greater conformational flexibility should have fewer intramolecular interactions than the more rigid regions. Therefore, fewer intramolecular interactions must be disrupted in order to release pairs of fragment ions (N- and C-terminal products) when a particular backbone bond is cleaved, thus accounting for higher UVPD yields. Moreover, as mentioned above absorption cross sections of different structural elements of proteins are known to vary in solution,[64] thus potentially translating to variations in local absorptivities in the gas phase.

Upon comparison of the backbone fragmentation trends for apo-DHFR and DHFR·NADPH, the most notable enhancement in fragmentation occurs in the region of the M20 loop (particularly backbone cleavages associated with residues 12−25) as well as from residues 37 to 41 (Figures 1a and 2a). For the same comparison, significant suppression of UVPD fragmentation occurred in the adenosine binding domain (ABD) in the loop regions from residues 51 to 54, 62 to 65, and 84 to 88. There were only a few backbone cleavages in the ABD that were enhanced for the DHFR·NADPH complex relative to DHFR (cleavages adjacent to residues 55, 56, 95, and 96). Some suppression of UVPD occurred in the helices of the ABD (namely in the C, E, and F helices), most notably adjacent to residues 102−104 in the F-helix. This suggests that NADPH binding causes a conformational shift of the M20 loop as well as in the ABD, specifically in the loop region containing residues 62−65. These changes in the UVPD pattern parallel some of the insights drawn by Sawaya et al., whom reported the most in-depth crystallographic analysis of the loop and subdomain movements of DHFR and its NADPH complexes.[51] They mapped the binding of the adenosine portion of NADPH to the ABD as well as the shift the M20 loop from a disordered or open conformation to a closed conformation upon NADPH binding.[51] Sawaya et al. also reported that the transition from an open to closed state resulted in disruption of hydrogen bonds between residues N23 and S148.[51] While a large change in the UVPD cleavage pattern is not observed next to residue S148, there is a substantial enhancement in backbone cleavage adjacent to residues L24 and P25 which directly neighbor N23. Also notable is the lack of significant changes in cleavage of the backbone sites in the F-G loop which are presumed to maintain hydrogen bonds with the M20 loop in the DHFR·NADPH complex.[51]

Sawaya et al. determined that apo-DHFR and its DHFR·MTX complex had similar crystal structures overall; however, the M20 loop was disordered in the apo-DHFR structure, but upon binding MTX the M20 loop adopted a more stable open conformation.[51] The main interaction between DHFR and MTX was purported to involve the (*p*-aminobenzoyl)glutamate (pABG) section of MTX and helix B of DHFR (see structural guide in Supporting Information, Figure 1) which arose from significant hydrophobic interactions.[51] Such interactions are anticipated to be diminished in the gas phase, thus rationalizing both the lower retention of MTX in the fragment ions produced upon UVPD of the binary DHFR·MTX and ternary DHFR·MTX·NADPH complexes as well as the relatively modest amount of change in fragmentation between the apo-DHFR and DHFR·MTX complexes (Figure 1b). However, there are still some notable enhancements in UVPD fragmentation for the DHFR·MTX complex relative to apo-DHFR. These changes are most prominent in the M20 loop, specifically enhancements in backbone cleavage adjacent to residues 17−18 and in helix B (next to residues 34, 37, 38, 40, and 41). These changes in UVPD within the M20 loop are rationalized based on an ordering of the loop upon MTX binding and the interaction of helix B with MTX. In comparison to the DHFR·NADPH complex, there is little suppression of backbone cleavage of DHFR in the DHFR·MTX complex and virtually no changes in UVPD in the ABD region (which is remote from the MTX binding site based on the crystal structure).

Upon inspection of the UVPD fragmentation trends for the ternary DHFR·MTX·NADPH complex (Figures 1c and 2c,d), there is a significant increase in the number of backbone cleavage sites suppressed or enhanced for the ternary complex in comparison to apo-DHFR or the binary complexes. Most of the changes mirror those already noted upon the binding of NADPH, such as suppression of fragmentation in the ABD and enhancement of fragmentation in the M20 loop. However, there are new enhancements when both ligands are affiliated with DHFR. These new regions of enhancement occur in the F-G and G-H loops and in the central β-sheet of the enzyme.

It has been suggested previously that the ternary DHFR·MTX·NADPH complex mimics and exhibits properties similar to that of the active protein transition state for the reduction of dihydrofolate (DHF) to tetrahydrofolate (THF).[51] Upon reduction of DHF, the M20 loop adopts an occluded state which results in disruption of hydrogen bonds between residues G121 and D122 from the F-G loop and residues G15 and M16 from the M20 loop.[51] Additionally upon this M20 loop transition, residue S148 from the G-H loop reforms a hydrogen bond to N23.[51] Other conformational changes occur during this transition-like state, including binding of NADPH and a twisting of the β-sheet between strands A and E. These conformational changes are mirrored by large enhancement of backbone fragmentation upon UVPD, spanning both the F-G loop (next to residues 115, 116, 119−123, 125, 127−130) and G-H loop (next to residues 141−150) and with a lower degree of enhancement of fragmentation in the M20 loop (residues 14−16, 18−20, and 22). This low enhancement of UVPD in the M20 loop suggests that the M20 loop may be much less dynamic and instead maintains a more closed and rigid conformation. A small amount of suppression of fragmentation is also observed adjacent to residues 24 and 25 in the M20 loop. Interestingly, as noted above for the binary DHFR·NADPH complex the cleavage adjacent to these residues (24 and 25) was enhanced, presumably because the hydrogen bond between S148 and N23 was disrupted upon NADPH binding. All of these changes from UVPD tracked well with the transition-state mechanism of DHFR discussed above. While that transition-state explanation evolved from a crystallographic analysis of solid-state (static) structures,[50] the UVPD trends offer a dynamic depiction dependent on disruption and formation of hydrogen bonds or other electrostatic interactions that influence the propensity for backbone cleavages upon UVPD. There are also compelling changes in UVPD fragmentation occurring in the region of DHFR that directly contacts the MTX ligand. Certain backbone cleavages increased

DOI: 10.1021/jacs.5b04628
J. Am. Chem. Soc. 2015, 137, 9128−9135

in helix B (adjacent to residues 29, 32, and 34), whereas there was a significant suppression of backbone cleavages in the ABD region nearest the MTX binding site (next to residues 52, 53 and 55−59). This is suggestive of a stronger binding interaction occurring in the ternary DHFR·MTX·NADPH complex in comparison to the DHFR·MTX binary complex discussed above.

The pattern and relative abundance of ligand-containing (holo) sequence ions produced upon UVPD is displayed as a function of the backbone cleavage site in Figure 3 and is classified as N- or C-terminal ions. These types of maps are useful for discerning the location of the ligands upon dissociation of the noncovalent protein−ligand complexes. The identified holo ions represent a significant portion of the fragment abundance per residue and sometimes are responsible for 100% of the ion current affiliated with backbone cleavages at a particular residue (Supporting Information, Figure 6). As expected, those fragment ions that retain NADPH for the DHFR·NADPH complex differ from those that retain MTX for the DHFR·MTX complex, an outcome anticipated based on the different binding sites of each ligand. For example, the NADPH ligand is known to interact with residues in the M20 loop as well as those found in the ABD based on the extensive array of N- and C-terminal holo fragment ions that contain these same stretches of amino acids. These amino acids are highlighted in purple in the space-filled model of DHFR in Figure 4 and include residues 13, 14, 16−18, 59, 75, 77, 80−84,

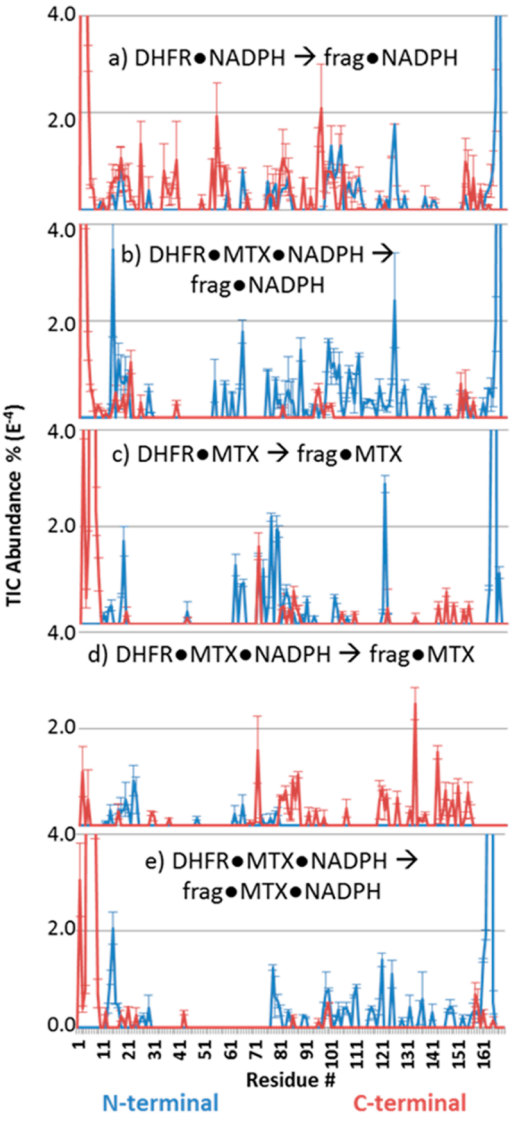

Figure 3. Plots of the N-terminal (blue) and C-terminal (red) holo fragment ions shown relative to the backbone cleavage site produced upon UVPD of DHFR·NADPH, DHFR·MTX, and DHFR·NADPH·MTX complexes, including those fragment ions retaining NADPH arising from (a) DHFR·NADPH and (b) DHFR·NADPH·MTX, those fragment ions retaining MTX arising from (c) DHFR·MTX and (d) DHFR·NADPH·MTX, and those fragment ions retaining both MTX and NADPH arising from (e) DHFR·NADPH·MTX. The 9+ charge state was selected for all experiments.

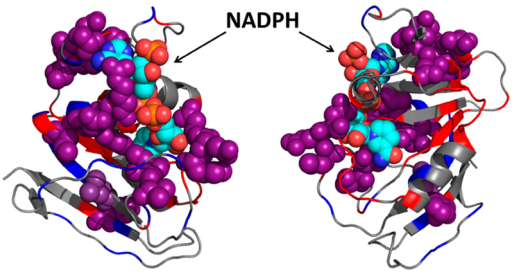

Figure 4. Space-filled model of NADPH (in blue/red/orange spheres) and the predicted interacting residues of DHFR (purple spheres) based on UVPD fragmentation. The residues of DHFR presumed to interact with NADPH correspond to those that show overlapping N- and C-termini holo ions from backbone cleavages upon UVPD. Other holo (NADPH-containing) fragment ions from the N-terminus are highlighted in blue, and other holo (NADPH-containing) fragment ions from the C-terminus are highlighted in red (nonspace filled).

98−101, 104, 112, 153, 159, and 162. This result is generally consistent with the interaction of NADPH with the M20 loop (residues 9−25) and the ABD (residues 38−107),[50] in particular involving polar contacts between DHFR (residues 7, 18, 19, 44−46, 63, 64, 96−98, and 102) and NADPH. (Polar contacts were found using PyMol with a 4 Å cutoff from analysis of crystal structure 1RX1.) The holo fragment ions produced upon UVPD do not overlay perfectly with the contact residues 7, 44−46, or 63−64 predicted from PyMol. However, there are both N- and C-terminal holo ions containing NADPH based on backbone cleavages adjacent to the predicted residues at 9 and 10 as well as 65−67. The proximity of these residues with those from the PyMol prediction provides compelling evidence that the holo fragment ions produced by UVPD reflect the NADPH binding site.

The MTX ligand was less consistently retained following UVPD, and thus fewer informative holo sequence ions were produced (Figure 3c). There are relatively few overlapping C- and N-terminal holo ions that are particularly diagnostic for elucidation of the ligand binding site. The MTX-containing fragment ions occurred from backbone cleavages adjacent to residues 43, 71, 81, 83, 85, and 122. There were also N- and C-terminal holo ions from backbone cleavages at residues 18 and 19. In general MTX is known to primarily interact with residues in the loop domain (1−37 and 108−159) and specifically with residues 5, 27, 52, 57, 94, and 100 based on polar contacts from crystal structure 1RG7.[50] The low frequency of holo fragment ions prohibited more detailed assessment of the MTX binding site based on the UVPD data.

UVPD of the ternary DHFR·NADPH·MTX complex resulted in an extensive array of NADPH-containing fragment

DOI: 10.1021/jacs.5b04628
J. Am. Chem. Soc. 2015, 137, 9128−9135

ions (Figure 3b,e) encompassing many of the same ones as observed for the DHFR·NADPH complex, with some exceptions. For the ternary DHFR·NADPH·MTX complex there are a more elaborate array of C-terminal ions and a stretch of missing C-terminal ions corresponding to cleavages adjacent to residues 34 to 38 that were notable for the binary DHFR·NADPH complex. The latter residues encompass or border helix B. Helix B is known to directly interact with MTX,[50] thus explaining the potential suppression of cleavage of those backbone sites upon UVPD of the ternary complex in the present study. Additionally, the production of MTX-containing N-terminal fragments arising from backbone cleavages from residues 13 to 23 was observed upon UVPD of the ternary DHFR·NADPH·MTX complex (Figure 3d,e) in addition to backbone cleavages from 9 to 12 and 17 to 19 previously noted upon UVPD of the binary DHFR·MTX complex. The enhancement in the number and variety of MTX-containing fragment ions for the ternary complex suggests modulation of MTX binding in conjunction with NADPH binding which causes the M20 loop (residues 9−25) to change conformation.

There is less noticeable overlap in the sequence ions that retain solely MTX or solely NADPH for the ternary DHFR·NADPH·MTX complexes relative to the corresponding holo sequence ions observed upon UVPD of the binary DHFR·NADPH and DHFR·MTX complexes (i.e., Figure 3a versus 3b,c versus 3d). For example, there are many more C-terminal ions that retain NADPH for DHFR·NADPH (Figure 3a) than for DHFR·NADPH·MTX (Figure 3b). In contrast, there are more N-terminal ions that retain MTX for DHFR·MTX (Figure 3c) than for DHFR·NADPH·MTX (Figure 3d). This may be explained by the fact that NADPH is mainly associated with the ABD which is largely composed of the middle of the N-terminal half of the protein, and MTX is known to interact with the helix B region of the loop domain, thus "splitting" the holo N-terminal ion current. In terms of the fragment ions that retain *both* ligands upon UVPD of the ternary DHFR·NADPH·MTX complexes, the N-terminal fragments showed significant overlap with the N-terminal NADPH-containing fragment ions from DHFR·NADPH (Figure 3a versus 3e). This results suggests that NADPH does not "migrate" significantly upon addition of the second ligand (MTX) nor does the UVPD process cause significant ligand rearrangement. The fragment ions that retained both MTX and NADPH upon UVPD of the DHFR·NADPH·MTX complexes are for the most part ones that mirror ones that retained NADPH or MTX alone. This complementarity is consistent with maintenance of the same networks of noncovalent interactions that retain NADPH at one region of the protein and MTX at another.

CONCLUSION

This study demonstrates the versatility of 193 nm UVPD for deciphering protein−ligand interactions in native-like ternary protein complexes. The retention of noncovalent interactions upon UV photoactivation allows the determination of ligand binding sites based on observation of ligand-containing (holo) product ions as well as suppression of backbone cleavages compared to the same backbone cleavages in the ligand-free (apo) protein. The UVPD trends correlate well with previously determined crystal structure information. Interpretation of the two pools of product ions (holo and apo) gives a more complete picture of the structural changes that DHFR undergoes upon NADPH and MTX binding. In particular, the changes in abundances of the holo and apo fragment ions reflect the conformational changes of DHFR that accompany the ligand binding events. The large array of holo fragment ions containing an N- or C-terminal portion of the protein and either NADPH, MTX or both NADPH and MTX ligands allowed the locations of each ligand to be determined in a manner that reflected the subdomain rotation and loop movements of DHFR upon interaction with the two ligands. The ability to examine ternary complexes (in addition to binary complexes and individual proteins) makes UVPD-MS a compelling new approach for addressing increasingly complicated questions in the arena of structural biology with numerous potential implications for studies of enzyme inhibitors and the drug discovery process. The potential sensitivity of UVPD to the impact of single point mutations on protein conformation is a related application that is currently underway.

ASSOCIATED CONTENT

Supporting Information

Supplemental Figures 1−7. These figures include labeled DHFR crystal structures, MS1 spectra, and MS2 UVPD spectra and deconvoluted spectra of the various DHFR binary and ternary complexes as well as graphical displays of N-terminal and C-terminal holo fragment ions, and B-factor plots. The Supporting Information is available free of charge on the ACS Publications website at DOI: 10.1021/jacs.5b04628.

AUTHOR INFORMATION

Corresponding Author

*jbrodbelt@cm.utexas.edu

Notes

The authors declare no competing financial interest.

ACKNOWLEDGMENTS

Funding from the NSF (CHE-1402753) and the Welch Foundation (F-1155) is acknowledged.

REFERENCES

(1) Konermann, L.; Vahidi, S.; Sowole, M. A. *Anal. Chem.* **2014**, *86*, 213−232.
(2) Pirrone, G. F.; Iacob, R. E.; Engen, J. R. *Anal. Chem.* **2015**, *87*, 99−118.
(3) Cammarata, M.; Lin, K.-Y.; Pruet, J.; Liu, H.; Brodbelt, J. *Anal. Chem.* **2014**, *86*, 2534−2542.
(4) Pan, J.; Han, J.; Borchers, C. H.; Konermann, L. *J. Am. Chem. Soc.* **2009**, *131*, 12801−12808.
(5) Novak, P.; Kruppa, G. H.; Young, M. M.; Schoeniger, J. *J. Mass Spectrom.* **2004**, *39*, 322−328.
(6) Wang, G.; Kaltashov, I. A. *Anal. Chem.* **2014**, *86*, 7293−7298.
(7) Stefanowicz, P.; Kijewska, M.; Szewczuk, Z. *Anal. Chem.* **2014**, *86*, 7247−7251.
(8) Bobst, C. E.; Kaltashov, I. A. *Anal. Chem.* **2014**, *86*, 5225−5231.
(9) Nagy, K.; Redeuil, K.; Rezzi, S. *Anal. Chem.* **2009**, *81*, 9365−9371.
(10) Robinson, E. W.; Leib, R. D.; Williams, E. R. *J. Am. Soc. Mass Spectrom.* **2006**, *17*, 1470−1480.
(11) Sharon, M.; Robinson, C. V. *Annu. Rev. Biochem.* **2007**, *76*, 167−193.
(12) Hall, Z.; Hernández, H.; Marsh, J. A.; Teichmann, S. A.; Robinson, C. V. *Structure* **2013**, *21*, 1325−1337.
(13) Zhang, Z.; Browne, S. J.; Vachet, R. W. *J. Am. Soc. Mass Spectrom.* **2014**, *25*, 604−613.
(14) Pan, J.; Han, J.; Borchers, C. H.; Konermann, L. *J. Am. Chem. Soc.* **2008**, *130*, 11574−11575.

DOI: 10.1021/jacs.5b04628
J. Am. Chem. Soc. 2015, 137, 9128−9135

(15) O'Brien, J. P.; Li, W.; Zhang, Y.; Brodbelt, J. S. *J. Am. Chem. Soc.* **2014**, *136*, 12920−12928.
(16) Hopper, J. T. S.; Oldham, N. J. *J. Am. Soc. Mass Spectrom.* **2009**, *20*, 1851−1858.
(17) Simmons, D. A.; Dunn, S. D.; Konermann, L. *Biochemistry* **2003**, *42*, 5896−5905.
(18) Wang, F.; Tang, X. *Biochemistry* **1996**, *35*, 4069−4078.
(19) Wright, P. J.; Zhang, J.; Douglas, D. J. *J. Am. Soc. Mass Spectrom.* **2008**, *19*, 1906−1913.
(20) Zhou, M.; Jones, C. M.; Wysocki, V. H. *Anal. Chem.* **2013**, *85*, 8262−8267.
(21) Breuker, K.; Brüschweiler, S.; Tollinger, M. *Angew. Chem., Int. Ed.* **2011**, *50*, 873−877.
(22) Yin, S.; Loo, J. A. *J. Am. Soc. Mass Spectrom.* **2010**, *21*, 899−907.
(23) Ly, T.; Julian, R. R. *J. Am. Chem. Soc.* **2010**, *132*, 8602−8609.
(24) Lermyte, F.; Konijnenberg, A.; Williams, J. P.; Brown, J. M.; Valkenborg, D.; Sobott, F. *J. Am. Soc. Mass Spectrom.* **2014**, *25*, 343−350.
(25) Modzel, M.; Stefanowicz, P.; Szewczuk, Z. *Rapid Commun. Mass Spectrom.* **2012**, *26*, 2739−2744.
(26) Cannon, J. R.; Cammarata, M. B.; Robotham, S. A.; Cotham, V. C.; Shaw, J. B.; Fellers, R. T.; Early, B. P.; Thomas, P. M.; Kelleher, N. L.; Brodbelt, J. S. *Anal. Chem.* **2014**, *86*, 2185−2192.
(27) Shaw, J. B.; Li, W.; Holden, D. D.; Zhang, Y.; Griep-Raming, J.; Fellers, R. T.; Early, B. P.; Thomas, P. M.; Kelleher, N. L.; Brodbelt, J. S. *J. Am. Chem. Soc.* **2013**, *135*, 12646−12651.
(28) Catherman, A. D.; Durbin, K. R.; Ahlf, D. R.; Early, B. P.; Fellers, R. T.; Tran, J. C.; Thomas, P. M.; Kelleher, N. L. *Mol. Cell. Proteomics* **2013**, *12*, 3465−3473.
(29) Skinner, O. S.; Catherman, A. D.; Early, B. P.; Thomas, P. M.; Compton, P. D.; Kelleher, N. L. *Anal. Chem.* **2014**, *86*, 4627−4634.
(30) Belov, M. E.; Damoc, E.; Denisov, E.; Compton, P. D.; Horning, S.; Makarov, A. A.; Kelleher, N. L. *Anal. Chem.* **2013**, *85*, 11163−11173.
(31) Syka, J. E. P.; Coon, J. J.; Schroeder, M. J.; Shabanowitz, J.; Hunt, D. F. *Proc. Natl. Acad. Sci. U. S. A.* **2004**, *101*, 9528−9533.
(32) Zubarev, R. A.; Kelleher, N. L.; McLafferty, F. W. *J. Am. Chem. Soc.* **1998**, *120*, 3265−3266.
(33) Heck, A. J. R. *Nat. Methods* **2008**, *5*, 927−933.
(34) Cammarata, M. B.; Brodbelt, J. S. *Chem. Sci.* **2015**, *6*, 1324−1333.
(35) Breuker, K.; McLafferty, F. W. *Proc. Natl. Acad. Sci. U. S. A.* **2008**, *105*, 18145−18152.
(36) Li, H.; Wongkongkathep, P.; Van Orden, S. L.; Ogorzalek Loo, R. R.; Loo, J. A. *J. Am. Soc. Mass Spectrom.* **2014**, *25*, 2060−2068.
(37) Zhang, H.; Cui, W.; Gross, M. L.; Blankenship, R. E. *FEBS Lett.* **2013**, *587*, 1012−1020.
(38) Cui, W.; Rohrs, H. W.; Gross, M. L. *Analyst* **2011**, *136*, 3854−3864.
(39) Warnke, S.; Baldauf, C.; Bowers, M. T.; Pagel, K.; von Helden, G. *J. Am. Chem. Soc.* **2014**, *136*, 10308−10314.
(40) Vahidi, S.; Stocks, B. B.; Konermann, L. *Anal. Chem.* **2013**, *85* (21), 10471−10478.
(41) Uetrecht, C.; Rose, R. J.; van Duijn, E.; Lorenzen, K.; Heck, A. J. R. *Chem. Soc. Rev.* **2010**, *39*, 1633−1655.
(42) Zhang, H.; Cui, W.; Gross, M. L. *Int. J. Mass Spectrom.* **2013**, *354*−*355*, 288−291.
(43) Cannon, J. R.; Kluwe, C.; Ellington, A.; Brodbelt, J. S. *Proteomics* **2014**, *14*, 1165−1173.
(44) Canon, F.; Milosavljević, A. R.; van der Rest, G.; Réfrégiers, M.; Nahon, L.; Sarni-Manchado, P.; Cheynier, V.; Giuliani, A. *Angew. Chem., Int. Ed.* **2013**, *52*, 8377−8381.
(45) Clarke, D. J.; Murray, E.; Hupp, T.; Mackay, C. L.; Langridge-Smith, P. R. R. *J. Am. Soc. Mass Spectrom.* **2011**, *22*, 1432−1440.
(46) Zhang, H.; Cui, W.; Wen, J.; Blankenship, R. E.; Gross, M. L. *Anal. Chem.* **2011**, *83*, 5598−5606.
(47) Li, H.; Wolff, J. J.; Van Orden, S. L.; Loo, J. A. *Anal. Chem.* **2014**, *86*, 317−320.
(48) Blackwell, A. E.; Dodds, E. D.; Bandarian, V.; Wysocki, V. H. *Anal. Chem.* **2011**, *83*, 2862−2865.
(49) Harvey, S. R.; Porrini, M.; Konijnenberg, A.; Clarke, D. J.; Tyler, R. C.; Langridge-Smith, P. R. R.; MacPhee, C. E.; Volkman, B. F.; Barran, P. E. *J. Phys. Chem. B* **2014**, *118*, 12348−12359.
(50) Huennekens, F. M. *Adv. Enzyme Regul.* **1994**, *34*, 397−419.
(51) Sawaya, M. R.; Kraut, J. *Biochemistry* **1997**, *36*, 586−603.
(52) Schnell, J. R.; Dyson, H. J.; Wright, P. E. *Annu. Rev. Biophys. Biomol. Struct.* **2004**, *33*, 119−140.
(53) Boehr, D. D.; McElheny, D.; Dyson, H. J.; Wright, P. E. *Science* **2006**, *313*, 1638−1642.
(54) Wang, Z.; Singh, P.; Czekster, C. M.; Kohen, A.; Schramm, V. L. *J. Am. Chem. Soc.* **2014**, *136*, 8333−8341.
(55) Wan, Q.; Bennett, B. C.; Wilson, M. A.; Kovalevsky, A.; Langan, P.; Howell, E. E.; Dealwis, C. *Proc. Natl. Acad. Sci. U. S. A.* **2014**, *111*, 18225−18230.
(56) Liu, C. T.; Francis, K.; Layfield, J. P.; Huang, X.; Hammes-Schiffer, S.; Kohen, A.; Benkovic, S. J. *Proc. Natl. Acad. Sci. U. S. A.* **2014**, *111*, 18231−18236.
(57) Hanoian, P.; Liu, C. T.; Hammes-Schiffer, S.; Benkovic, S. *Acc. Chem. Res.* **2015**, *48*, 482−489.
(58) Liu, C. T.; Layfield, J. P.; Stewart, R. J.; French, J. B.; Hanoian, P.; Asbury, J. B.; Hammes-Schiffer, S.; Benkovic, S. J. *J. Am. Chem. Soc.* **2014**, *136*, 10349−10360.
(59) Osborne, M. J.; Schnell, J.; Benkovic, S. J.; Dyson, H. J.; Wright, P. E. *Biochemistry* **2001**, *40*, 9846−9859.
(60) Hatse, S.; De Clercq, E.; Balzarini, J. *Biochem. Pharmacol.* **1999**, *58*, 539−555.
(61) Rajagopalan, P. T. R.; Zhang, Z.; McCourt, L.; Dwyer, M.; Benkovic, S. J.; Hammes, G. G. *Proc. Natl. Acad. Sci. U. S. A.* **2002**, *99*, 13481−13486.
(62) Li, R.; Sirawaraporn, R.; Chitnumsub, P.; Sirawaraporn, W.; Wooden, J.; Athappilly, F.; Turley, S.; Hol, W. G. J. *J. Mol. Biol.* **2000**, *295*, 307−323.
(63) Brunet, C.; Antoine, R.; Dugourd, P.; Canon, F.; Giuliani, A.; Nahon, L. *J. Chem. Phys.* **2013**, *138*, 064301.
(64) Tsai, C. S. *Biomacromolecules: Introduction to structure, function and informatics*; John Wiley & Sons: Hoboken, NJ, 2007.

DOI: 10.1021/jacs.5b04628
J. Am. Chem. Soc. 2015, 137, 9128−9135